Chapter 1

A Mathematical Theory of Climate Sensitivity or, How to Deal With Both Anthropogenic Forcing and Natural Variability?

Michael Ghil

Ecole Normale Supérieure, 75005 Paris, FRANCE, and
University of California, Los Angeles, CA 90095, USA
ghil@lmd.ens.fr[*]

Recent estimates of climate evolution over the coming century still differ by several degrees. This uncertainty motivates the work presented here. There are two basic approaches to apprehend the complexity of climate change: deterministically nonlinear and stochastically linear, i.e. the Lorenz and the Hasselmann approach. The grand unification of these two approaches relies on the theory of random dynamical systems. We apply this theory to study the random attractors of nonlinear, stochastically perturbed climate models. Doing so allows one to examine the interaction of internal climate variability with the forcing, whether natural or anthropogenic, and to take into account the climate system's non-equilibrium behavior in determining climate sensitivity.

This non-equilibrium behavior is due to a combination of nonlinear and random effects. We give here a unified treatment of such effects from the point of view of the theory of dynamical systems and of their bifurcations. Energy balance models are used to illustrate multiple equilibria, while multi-decadal oscillations in the thermohaline circulation illustrate the transition from steady states to periodic behavior. Random effects are introduced in the setting of random dynamical systems, which permit a unified treatment of both nonlinearity and stochasticity. The combined treatment of nonlinear and random effects is applied to a stochastically perturbed version of the classical Lorenz convection model.

Climate sensitivity is then defined mathematically as the derivative of an appropriate functional or other function of the systems state with respect to the bifurcation parameter. This definition is illustrated by using numerical results for a model of the El Niño–Southern Oscillation.

1.1. Introduction

The global climate system is composed of a number of subsystems — atmosphere, biosphere, cryosphere, hydrosphere and lithosphere — each of which has distinct characteristic times, from days and weeks to centuries and millennia. Each subsystem, moreover, has its own internal variability, all other things being constant, over a fairly broad range of time scales. These ranges overlap between one subsystem and another. The interactions between the subsystems thus give rise to climate variability on all time scales.

We outline here the rudiments of the way in which *dynamical systems theory* provides an understanding of this vast range of variability. Such an understanding proceeds through the study of successively more complex patterns of behavior. These spatio-temporal patterns are studied within narrower ranges of time scales, such as intraseasonal, interannual, interdecadal and multi-millennial. The main results of dynamical systems theory that have demonstrated their importance for the study of climate variability involve *bifurcation theory* and the *ergodic theory* of dynamical systems. More recently, the

---

[*]additional E-address: ghil@atmos.ucla.edu.

theory of random dynamical systems has made substantial contributions as well.

In the next section, we describe the climate systems dominant balance between incoming solar radiation, dominated by short waves, and outgoing terrestrial radiation, dominated by long waves. This balance is consistent with the existence of multiple equilibria of surface temperatures.

Such *multiple equilibria* are also present for other balances of climatic actions and reactions. Thus, on the intraseasonal time scale, the thermal driving of the mid-latitude westerly winds is countered by surface friction and mountain drag. Multiple equilibria typically arise from saddle-node bifurcations of the governing equations. Transitions from one equilibrium to another may result from small and random pushes — a typical case of minute causes having large effects in the long term.

In Sec. 1.3, we sketch the oceans overturning circulation between cold regions, where water is heavier and sinks, and warm regions, where it is lighter and rises. The effect of temperature on the water masses density and, hence, motion is in competition with the effect of salinity: density increases, through evaporation and brine formation, compete further with decreases in salinity and, hence, density through precipitation and river run-off. These competing effects can also give rise to two distinct equilibria.

In the present-day oceans, a *thermohaline* circulation prevails, in which the temperature effects dominate. In the remote past, about 50 Myr ago, a *halothermal* circulation may have obtained, with salinity effects dominating. In a simplified mathematical setting, these two equilibria arise by a pitchfork bifurcation that breaks the problems mirror symmetry. On shorter time scales, of decades-to-millennia, oscillations of intensity and spatial pattern in the thermohaline circulation seem to be the dominant mode of variability. We show how interdecadal oscillations in the oceans circulation arise by Hopf bifurcation.

In Sec. 1.4, we address the way that faster processes, modeled as random effects, can interact with the slower, nonlinear ones. The combined treatment of the nonlinear and stochastic processes can reveal amazingly fine structure in the climate systems behavior, but also — and rather surprisingly — add robustness and predictability to the results.

In Sec. 1.5, we discuss the way that climate sensitivity can be defined in the stochastic vs. the deterministic context. Concluding remarks follow in Sec. 1.6.

1.2. Energy-Balance Models and the Modeling Hierarchy

The concepts and methods of the theory of deterministic dynamical systems (Andronov and Pontryagin, 1937; Arnol'd, 1983; Guckenheimer and Holmes, 1983) have been applied first to simple models of atmospheric and oceanic flows, starting about fifty years ago (Lorenz, 1963; Stommel, 1961). More powerful computers now allow their application to fairly realistic and detailed models of the atmosphere, ocean, and the coupled atmosphereocean system. We start therefore by presenting such a hierarchy of models.

This presentation is interwoven with that of the successive bifurcations that lead from simple to more complex solution behavior for each climate model. Useful tools for comparing model behavior across the hierarchy and with observations are provided by ergodic theory (Eckmann and Ruelle, 1985; Ghil *et al.*, 2008a). Among these, advanced methods for the analysis and prediction of uni- and multivariate time series play an important role.

1.2.1. *Radiation balance and energy-balance models (EBMs)*

The concept of a modeling hierarchy in climate dynamics was introduced by Schneider and Dickinson (1974); it is discussed in greater detail by Ghil and Robertson (2000) and by

Dijkstra and Ghil (2005). At present, the best-developed hierarchy is for atmospheric models. These models were originally developed for weather simulation and prediction on the time scale of hours to days. Currently they serve in a stand-alone mode or coupled to oceanic and other models to address climate variability on all time scales.

The first rung of the modeling hierarchy for the atmosphere is formed by zero-dimensional (0-D) models, where the number of dimensions, from zero to three, refers to the number of independent space variables used to describe the model domain, i.e. to physical-space dimensions. Such 0-D models essentially attempt to follow the evolution of global surface-air temperature as a result of changes in global radiative balance:

$$c\frac{\mathrm{d}\bar{T}}{\mathrm{d}t} = R_\mathrm{i} - R_\mathrm{o}, \tag{1.1a}$$

$$R_\mathrm{i} = \mu Q_0\{1 - \alpha(\bar{T})\}, \tag{1.1b}$$

$$R_\mathrm{o} = \sigma m(\bar{T})(\bar{T})^4. \tag{1.1c}$$

Here R_i and R_o are incoming solar radiation and outgoing terrestrial radiation. The heat capacity c is that of the global atmosphere, plus that of the global ocean or some fraction thereof, depending on the time scale of interest: one might only include in c the ocean mixed layer when interested in subannual time scales but the entire ocean when studying paleoclimate.

The rate of change of $\bar{T}$ with time t is given by $\mathrm{d}\bar{T}/\mathrm{d}t$, while Q_0 is the solar radiation received at the top of the atmosphere, σ is the Stefan-Boltzmann constant, and m is an insolation parameter, equal to unity for present-day conditions. To have a closed, self-consistent model, the planetary reflectivity or albedo α and grayness factor m have to be expressed as functions of $\bar{T}$; $m = 1$ for a perfectly black body and $0 < m < 1$ for a grey body like planet Earth.

There are two kinds of one-dimensional (1-D) atmospheric models, for which the single spatial variable is latitude or height, respectively. The former are so-called energy-balance models (EBMs), which consider the generalization of

the model (2.1) for the evolution of surface-air temperature $T = T(x, t)$, say,

$$c(x)\frac{\partial \bar{T}}{\partial t} = R_\mathrm{i} - R_\mathrm{o} + D. \tag{1.2}$$

Here the terms on the right-hand side can be functions of the meridional coordinate x (latitude, co-latitude, or sine of latitude), as well as of time t and temperature T. The horizontal heat-flux term D expresses heat exchange between latitude belts; it typically contains first and second partial derivatives of T with respect to x. Hence the rate of change of local temperature T with respect to time also becomes a partial derivative, $\partial \bar{T}/\partial t$. Such models were introduced independently by Budyko (1969) and by Sellers (1969).

The first striking results of theoretical climate dynamics were obtained in showing that Eq. (1.2) could have two stable steady-state solutions, depending on the value of the insolation parameter μ, cf. Eq. (1.1b). This multiplicity of stable steady states, or physically possible climates of our planet, can be explained, in its simplest form, in the 0-D model given by Eq. (1.1).

The physical explanation resides in the fact that — for a fairly broad range of μ-values around $\mu = 1.0$ — the curves for R_i and R_o as a function of $\bar{T}$ intersect in 3 points. One of these points corresponds to the present climate (highest $\bar{T}$-value), and another one to an ice-covered planet (lowest $\bar{T}$-value); both of these are stable, while the third one (intermediate $\bar{T}$-value) is unstable. To obtain this result, it suffices to make two assumptions: (i) that $\alpha = \alpha(\bar{T})$ is a piecewise-linear function of $\bar{T}$, with high albedo at low temperature, due to the presence of snow and ice, and low albedo at high $\bar{T}$, due to their absence; and (ii) that $m = m(\bar{T})$ is a smooth, increasing function of $\bar{T}$ that attempts to capture in its simplest from the greenhouse effect of trace gases and water vapor.

The bifurcation diagram of a 1-D EBM, like the one of Eq. (1.2), is shown in Fig. 1.1. It displays the model's mean temperature $\bar{T}$ as a function of the fractional change μ in the inso-

4   M. Ghil

lation $Q = Q(x)$ at the top of the atmosphere. The S-shaped curve in the figure arises from two back-to-back *saddle-node bifurcations*.
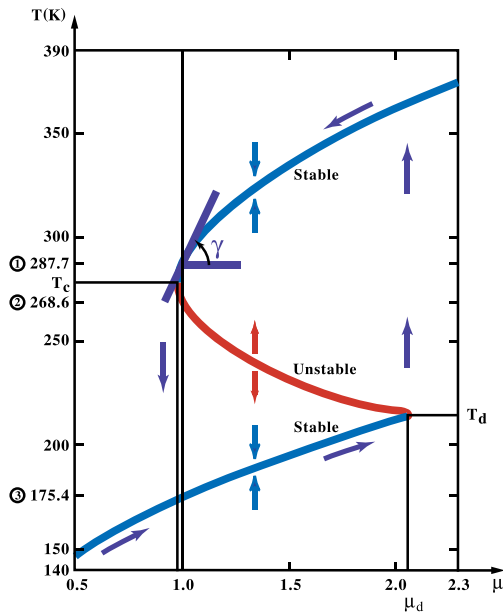

Fig. 1.1. Bifurcation diagram for the solutions of an energy-balance model (EBM), showing the global-mean temperature $\bar{T}$ vs. the fractional change μ of insolation at the top of the atmosphere. The arrows pointing up and down at about $\mu = 1.4$ indicate the stability of the branches: towards a given branch if it is stable and away if it is unstable. The other arrows show the hysteresis cycle that global temperatures would have to undergo for transition from the upper stable branch to the lower one and back. The angle γ gives the measure of the present climates sensitivity to changes in insolation. [After Ghil and Childress (1987) with permission from Springer-Verlag.]

The normal form of the first one is

$$\dot{X} = \mu - X^2. \tag{1.3}$$

Here X stands for a suitably normalized form of $\bar{T}$ and $\dot{X}$ is the rate of change of X, while μ is a parameter that measures the stress on the system, in particular a normalized form of the insolation parameter.

The uppermost branch corresponds to the steady-state solution $X = +\mu^{1/2}$ of Eq. (1.3) and it is stable. This branch matches rather well

Earth's present-day climate for $\mu = 1.0$; more precisely the steady-state solution $T = T(x; \mu)$ of the full 1-D EBM (not shown) matches closely the annual mean temperature profile from instrumental data over the last century.

The intermediate branch starts out at the left as the second solution, $X = -\mu^{1/2}$, of Eq. (1.3) and it is unstable. It blends smoothly into the upper branch of a coordinate-shifted and mirror-reflected version of Eq. (1.3), say

$$\dot{X} = \mu - X^2. \tag{1.4}$$

This branch, $X = X_0 + (\mu_0 - \mu)^{1/2}$, is also unstable. Finally, the lowermost branch in Fig. 1.1 is the second steady-state solution of Eq. (1.4), $X = X_0(\mu_0 - \mu)^{1/2}$, and it is stable, like the uppermost branch. The lowermost branch corresponds to an ice-covered planet at the same distance from the Sun as Earth.

The fact that the upper-left bifurcation point (μ_c, T_c) in Fig. 1.1 is so close to present-day insolation values created great concern in the climate dynamics community in the mid-1970s, when these results were obtained. Indeed, much more detailed computations (see below) confirmed that a reduction of about 2–5% of insolation values would suffice to precipitate Earth into a deep freeze. The great distance of the lower-right bifurcation point (μ_d, T_d) from present-day insolation values, on the other hand, suggests that one would have to nearly double atmospheric opacity, say, for the Earth's climate to jump back to more comfortable temperatures.

The results here follow Ghil (1976). Held and Suarez (1974) and North North (1975) obtained similar results, and a detailed comparison between EBMs appears in Chapter 10 of Ghil and Childress (1987).

1.2.2. *Other atmospheric processes and models*

The 1-D atmospheric models in which the details of radiative equilibrium are investigated with respect to a height coordinate z (geometric height, pressure, etc.) are often called

radiative-convective models (Ramanathan and Coakley, 1978). This name emphasizes the key role that convection plays in vertical heat transfer. While these models preceded historically EBMs as rungs on the modeling hierarchy, it was only recently shown that they, too, could exhibit multiple equilibria (Li et al., 1997). The word (stable) equilibrium, here and in the rest of this article, refers simply to a (stable) steady state of the model, rather than a to true thermodynamic equilibrium.

Two-dimensional (2-D) atmospheric models are also of two kinds, according to the third space coordinate that is not explicitly included. Models that resolve explicitly two horizontal coordinates, on the sphere or on a plane tangent to it, tend to emphasize the study of the dynamics of large-scale atmospheric motions. They often have a single layer or two. Those that resolve explicitly a meridional coordinate and height are essentially combinations of EBMs and radiative-convective models and emphasize therewith the thermodynamic state of the system, rather than its dynamics.

Yet another class of horizontal 2-D models is the extension of EBMs to resolve zonal, as well as meridional surface features, in particular land-sea contrasts. We shall see in Sec. 1.3.2 how such a 2-D EBM is used, when coupled to an oceanic model.

Schneider and Dickinson (1974) and Ghil and Robertson (2000) discuss additional types of 1-D and 2-D atmospheric models and give references to these and to the types discussed above, along with some of their main applications. Finally, to encompass and resolve the main atmospheric phenomena with respect to all three spatial coordinates, general circulation models (GCMs) occupy the pinnacle of the modeling hierarchy.

The dependence of mean zonal temperature on the insolation parameter μ (the normalized "solar constant") — as obtained for 1-D EBMs and shown in Fig. 1.1 here — was confirmed, to the extent possible, by using a simplified GCM,

coupled to a swamp ocean model. More precisely, forward integrations with a GCM cannot confirm the presence of the intermediate, unstable branch. Nor was it possible in the mid-70s, when this numerical experiment was done, to reach the deep-freeze stable branch, because of the GCMs computational limitations. But the parabolic shape of the upper, present-daylike branch near the upper-left bifurcation point in our figure, cf. Eq. (1.3), was well supported by the GCM simulations.

Ghil and Robertson (2000) also describe the separate hierarchies that have grown over the last quarter-century in modeling the ocean and the coupled oceanatmosphere system. More recently, an overarching hierarchy of earth-system models that encompass all the subsystems of interest, atmosphere, biosphere, cryosphere, hydrosphere and lithosphere has been developing. Eventually, the partial results about each subsystems variability, outlined in this section and the next one, will have to be verified from one rung to the next of the Earth-system modeling hierarchy.

1.3. Oscillations in the Oceans' Thermohaline Circulation

1.3.1. *Theory and simple models*

Historically, the thermohaline circulation (THC) was first among the climate systems major processes to be studied using a very simple mathematical model. Stommel (1961) formulated a two-box model and showed that it possessed multiple equilibria.

A sketch of the Atlantic Oceans THC and its interactions with the atmosphere and cryosphere on long time scales is shown in Fig. 1.2. These interactions can lead to climate oscillations with multi-millennial periods, such as the Heinrich events, and are summarized in the figures caption. An equally schematic view of the global THC is provided by the widely known "conveyor belt" diagram. The latter diagram captures greater horizontal, 2-D detail but

M. Ghil

it does not commonly include the THCs inter-actions with water in both its gaseous and solid phases, which our Fig. 1.2 here does include.
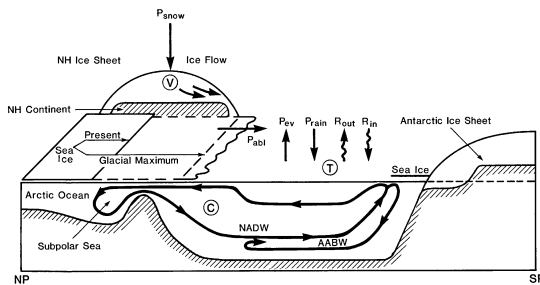

Fig. 1.2.   Diagram of an Atlantic meridional cross section from North Pole (NP) to South Pole (SP), showing mechanisms likely to affect the thermohaline circulation (THC) on various time-scales. Changes in the radiation balance $R_{\mathrm{in}} - R_{\mathrm{out}}$ are due, at least in part, to changes in extent of Northern Hemisphere (NH) snow and ice cover V, and to how these changes affect the global temperature T; the extent of Southern Hemisphere ice is assumed constant, to a first approximation. The change in hydrologic cycle expressed in the terms $P_{\mathrm{rain}} - P_{\mathrm{evap}}$ for the ocean and $P_{\mathrm{snow}} - P_{\mathrm{abl}}$ for the snow and ice is due to changes in ocean temperature. Deep-water formation in the North Atlantic Subpolar Sea (North Atlantic Deep Water: NADW) is affected by changes in ice volume and extent, and regulates the intensity C of the THC; changes in Antarctic Bottom Water (AABW) formation are neglected in this approximation. The THC intensity C in turn affects the systems temperature, and is also affected by it. [After Ghil *et al.* (1987) with permission from Springer-Verlag.]

Basically, the THC is due to denser water sinking, lighter water rising, and water-mass continuity closing the circuit through near-horizontal flow between the areas of rising and sinking. The effects of temperature and salinity on the ocean waters density, $\rho = \rho(T,S)$, oppose each other: the density ρ *decreases* as T increases and it *increases* as S increases. It is these two effects that give the *thermohaline* circulation its name, from the Greek words for T and S. In high latitudes, ρ increases as the water loses heat to the air above and, if sea ice is formed, as the water underneath is enriched in brine. In low latitudes, ρ increases due to evaporation but decreases due to sensible heat flux into the ocean.

For the present climate, the temperature effect is stronger than the salinity effect, and ocean water is observed to sink in certain areas of the high-latitude North Atlantic and Southern Ocean — with very few and limited areas of deep-water formation elsewhere — and to rise everywhere else. Thus, in a *thermohaline* regime, T is more important than S and hence comes before it. During some remote geological times, deep water may have formed in the global ocean near the equator; such an overturning circulation of opposite sign to that prevailing today has been dubbed *halothermal*, S before T. The quantification of the relative effects of T and S on the oceanic water masses buoyancy in high and low latitudes is far from complete, especially for paleocirculations; the association of the latter with salinity effects that exceed the thermal ones (Kennett and Stott, 1991) is thus rather tentative.

To study the reversal of the abyssal circulation, due to the opposite effects of T and S, Stommel considered a two-box model, with two pipes connecting the two boxes. He showed that the system of two nonlinear, coupled ordinary differential equations that govern the temperature and salinity differences between the two well-mixed boxes has two stable steady-state solutions; these two steady states are distinguished by the direction of flow in the upper and lower pipe. Stommel's paper was primarily concerned with distinct local convection regimes, and hence vertical stratifications, in the North Atlantic and the Mediterranean or the Red Sea, say. Today, we mainly think of one box as representing the low latitudes and the other one the high latitudes in the global THC (Marotzke, 2000).

The next step in the hierarchical modeling of the THC is that of 2-D meridional plane models, in which the temperature and salinity fields are governed by coupled nonlinear partial differential equations with two independent space variables, latitude and depth, say. Given boundary conditions for such a model that are symmetric

about the Equator, as the equations themselves are, one expects a symmetric solution, in which water either sinks near the poles and rises everywhere else (thermohaline) or sinks near the Equator and rises everywhere else (halothermal). These two symmetric solutions would correspond to the two equilibria of Stommel's box model of 1961.

In fact, *symmetry breaking* can occur, leading gradually from a symmetric two-cell circulation to an antisymmetric one-cell circulation. In between, all degrees of dominance of one cell over the other are possible. A situation lying somewhere between the two seems to resemble most closely the meridional overturning diagram of the Atlantic Ocean in Fig. 1.2.

This symmetry breaking can be described by a *pitchfork bifurcation*:

$$\dot{X} = \mu - X^3. \qquad (1.5)$$

Here X stands for the amount of asymmetry in the solution, so that $X = 0$ is the symmetric branch, and μ is a parameter that measures the stress on the system, in particular a normalized form of the buoyancy flux at the surface. For $\mu < 0$ the symmetric branch is stable, while for $\mu > 0$ the two branches $X = \pm\mu^{1/2}$ inherit its stability.

In the 2-D THC problem, the left cell dominates on one branch, while the right cell dominates on the other: for a given value of μ, the two stable steady-state solutions — on the $\{X = +\mu^{1/2}\}$ branch and on the $\{X = -\mu^{1/2}\}$ branch — are mirror images of each other. The idealized THC in Fig. 1.2, with the North Atlantic Deep Water extending to the Southern Oceans polar front, corresponds to one of these two branches. In theory, therefore, a mirror-image circulation, with the Antarctic Bottom Water extending to the North Atlantics polar front, is equally possible.

1.3.2. *Bifurcation diagrams for GCMs*

Bryan (1986) was the first to document transition from a two-cell to a one-cell circulation in a simplified ocean GCM with idealized, symmetric forcing. Results of coupled oceanatmosphere GCMs, however, have led to questions about the realism of more than one stable THC equilibrium. The situation with respect to the THCs pitchfork bifurcation (1.5) is thus subtler than it was with respect to Fig. 1.1 for radiative equilibrium. In the previous section, atmospheric GCMs confirmed essentially the EBM results; the results obtained in climbing the rungs of the modeling hierarchy for the THC are still in need of further clarification.

Internal variability of the THC with smaller and more regular excursions than the huge and totally irregular jumps associated with bistability was studied intensively in the late 1980s and the 1990s. These studies placed themselves on various rungs of the modeling hierarchy, from box models through 2-D models and all the way to ocean GCMs. A summary of the different kinds of oscillatory variability found in the latter appears in Table 1.1. Such oscillatory behavior seems to match more closely the instrumentally recorded THC variability, as well as the paleoclimatic records for the recent geological past, than bistability.

The (multi)millennial oscillations interact with variability in the surface features and processes shown in Fig. 1.2. Chen and Ghil (1996), in particular, studied some of the interactions between atmospheric processes and the THC. They used a so-called hybrid coupled model, namely a (horizontally) 2-D EBM, coupled to a rectangular-box version of the North Atlantic rendered by a low-resolution ocean GCM. This hybrid models regime diagram is shown in Fig. 1.3(a). A steady state is stable for high values of the coupling parameter or of the EBMs diffusion parameter d. Interdecadal oscillations with a period of 40–50 years are self-sustained and stable for low values of these parameters.

The self-sustained THC oscillations in question are characterized by a pair of vortices of opposite sign that grow and decay in quadrature with each other in the oceans upper layers.

8   M. Ghil

Table 1.1.   Oscillations in the oceans' thermohaline circulation.

Time scale	Phenomena	Mechanism[a]
Decadal	· Local migration of surface anomalies in the northwest corner of the ocean basin · Gyre advection in mid-latitudes	· Localized surface density anomalies due to surface coupling · Gyre advection
Centennial	Loop-type, meridional circulation	Conveyor-belt advection of density anomalies
Millennial	Relaxation oscillation, with "flushes" and superimposed decadal fluctuations	Bottom water warming, due to strong braking effect of salinity forcing

[a] Full references to these mechanisms are given in Ghil (1994).

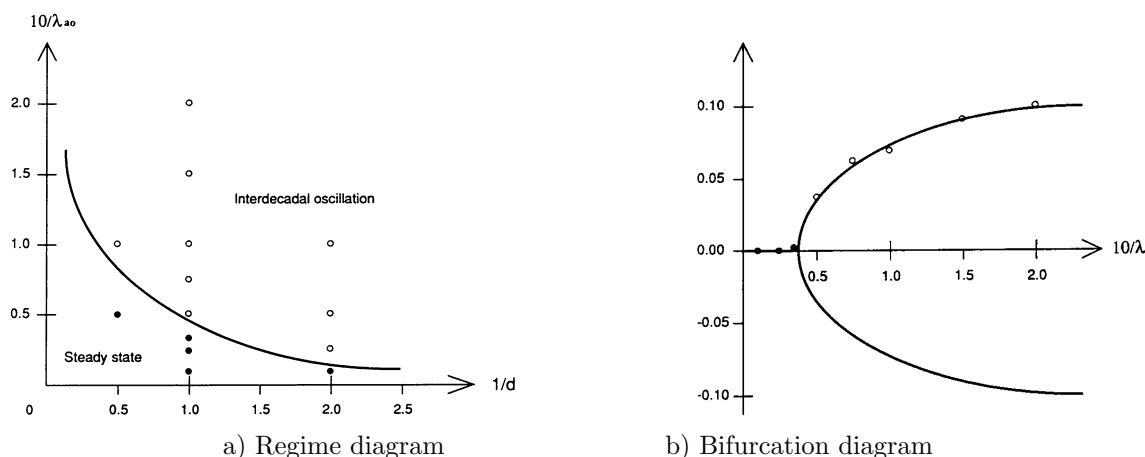a) Regime diagram   b) Bifurcation diagram

Fig. 1.3.   Dependence of THC solutions on two parameters in a hybrid coupled model; the two parameters are the atmosphere-ocean coupling coefficient λ_{ao} and the atmospheric thermal diffusion coefficient d. (a) Schematic regime diagram. The full circles stand for the models stable steady states, the open circles for stable limit cycles, and the solid curve is the estimated neutral stability curve between the former and the latter. (b) Hopf bifurcation curve at fixed d = 1.0 and varying λ_{ao}; this curve was obtained by fitting a parabola to the models numerical-simulation results, shown as full and open circles. [From Chen and Ghil (1996) with permission from the American Meteorological Society.]

Their centers follow each other anti-clockwise through the northwestern quadrant of the models rectangular domain. Both the period and the spatio-temporal characteristics of the oscillation are thus rather similar to those seen in a fully coupled GCM with realistic geometry. The transition from a stable equilibrium to a stable limit cycle, via Hopf bifurcation, in this hybrid coupled model, is shown in Fig. 1.3(b).

1.4. Randomness and Nonlinearity

1.4.1. *What to expect*

The geometric (Arnol'd, 1983; Guckenheimer and Holmes, 1983) and the ergodic (Eckmann and Ruelle, 1985) theory of dynamical systems

represent significant achievements of the 20th century. The foundations of the stochastic calculus in its second half (Doob, 1953) also led to the birth of a rigorous theory of time-dependent random phenomena. Historically, theoretical developments in climate dynamics have been largely motivated by these two complementary approaches, based on the work of E. N. Lorenz and that of K. Hasselmann (Lorenz, 1963; Hasselmann, 1976), respectively.

It now seems clear that these two approaches complement, rather than exclude each other. Incomplete knowledge of small-, subgrid-scale processes, as well as computational limitations will always require one to account for these processes in a stochastic way. As a result of

sensitive dependence on initial data and on parameters, numerical weather forecasts, as well as climate projections are both expressed these days in probabilistic terms. In addition to the intrinsic challenge of addressing the nonlinearity along with the stochasticity of climatic processes, it is thus more convenient — and becoming more and more necessary — to rely on a model's (or set of models') *probability density function* (PDF) rather than on its individual, point-wise simulations or predictions.

We summarize here results on the surprisingly complex statistical structure that characterizes stochastic nonlinear systems. This complex structure does provide meaningful physical information that is not described by the PDF alone; it lives on a *random attractor*, which extends the concepts of a *strange attractor* and of the *invariant measure* that is supported by it, from the deterministic to the stochastic framework.

1.4.2. *What one finds*

On the road to including random effects, one needs to realize first that the climate system — as well as any of its subsystems, and on any time scale — is not closed: it exchanges energy, mass and momentum with its surroundings, whether other subsystems or the interplanetary space and the solid earth. The typical applications of dynamical systems theory to climate variability so far have only taken into account exchanges that are constant in time, thus keeping the model — whether governed by ordinary, partial or other differential equations — *autonomous*; i.e., the models had coefficients and forcings that were constant in time.

Succinctly, one can write such a system as

$$\dot{\mathbf{X}} = \mathbf{f}(\mathbf{X}; \boldsymbol{\mu}), \qquad (1.6)$$

where $\mathbf{X}$ now may stand for any state vector or climate field, while $\mathbf{f}$ is a smooth function of $\mathbf{X}$ and of the vector of parameters $\boldsymbol{\mu}$, but does not depend explicitly on time. This characteristic of

being autonomous greatly facilitated the analysis of model solutions' properties. For instance, two distinct trajectories, $\mathbf{X}_1(t)$ and $\mathbf{X}_2(t)$, of a well-behaved, smooth autonomous system cannot pass through the same point in phase space, which helps describe the systems phase portrait. So does the fact that we only need to consider the behavior of solutions $\mathbf{X}(t)$ as we let time t tend to $+\infty$: the resulting sets of points are — possibly multiple — equilibria, periodic solutions, and chaotic sets. In the language of dynamical systems theory, these are called, respectively: *fixed points, limit cycles,* and strange attractors.

We know only too well, however, that the seasonal cycle plays a key role in climate variability on many time scales, while orbital forcing is crucial on the Quaternary time scales of many millennia, and now anthropogenic forcing is of utmost importance on interdecadal time scales. How can one take into account such time-dependent forcings, and analyze the non-autonomous systems, written succinctly as

$$\dot{\mathbf{X}} = \mathbf{f}(\mathbf{X}, t; \boldsymbol{\mu}), \qquad (1.7)$$

to which they give rise? In Eq. (1.7), the dependence of $\mathbf{f}$ on t may be periodic, $\mathbf{f}(\mathbf{X}, t + P) = \mathbf{f}(\mathbf{X}, t)$, as in various El Niño–Southern Oscillation (ENSO) models, where the period $P = 12$ months, or monotone, $\mathbf{f}(\mathbf{X}, t + \tau) \geq \mathbf{f}(\mathbf{X}, t)$ for $\tau \geq 0$, as in studying scenarios of anthropogenic climate forcing.

To illustrate the fundamental character of the distinction between an autonomous system like (1.6) and a non-autonomous one like (1.7), consider the simple scalar version of these two equations:

$$\dot{X} = -\beta X, \qquad (1.8)$$

and

$$\dot{X} = -\beta X + \gamma t, \qquad (1.9)$$

respectively. We assume that both systems are dissipative, i.e. $\beta > 0$, and that the forcing is monotone increasing, $\gamma \geq 0$, as would be the case for anthropogenic forcing in the industrial

era. Lorenz (1963) pointed out the key role of dissipativity in giving rise to strange, but attracting solution behavior, while Ghil and Childress (1987) emphasized its importance and pervasive character in climate dynamics. Clearly the only attractor for the solutions of Eq. (1.8), given any initial point $X(0) = X_0$, is the fixed point $X = 0$, attained as $t \to +\infty$.

For the non-autonomous case of Eq. (1.9), though, this *forward-in-time approach* yields blow-up as $t \to +\infty$, for any initial point. To make sense of what happens in the case of time-dependent forcing, one introduces instead the *pullback approach*, in which solutions are allowed to still depend on the time t at which we observe them, but also on a time s from which the solution is started, $X(s) = X_0$; presumably $s \ll t$. With this little change of approach, one can easily verify that

$$|X(s, t; X_0) - \mathcal{A}(t)| \to 0 \quad \text{as} \quad s \to -\infty, \tag{1.10}$$

for all t and X_0, where

$$\mathcal{A}(t) = \frac{\gamma(t - 1/\beta)}{\beta}. \tag{1.11}$$

We thus obtain, in this pullback sense, the intuitively obvious result that the solutions, if started far enough in the past, all approach the attractor set $\mathcal{A}(\omega)$, which has a linear growth in time and thus follows the linear forcing.

Let us return now to the more general, nonlinear case of Eq. (1.7) and add not only deterministic time dependence $\mathbf{f}(\mathbf{X}, t)$, but also random forcing (Ledrappier and Young, 1988; Arnold, 1998),

$$d\mathbf{X} = \mathbf{f}(\mathbf{X}, t)dt + \mathbf{g}(\mathbf{X})d\eta, \tag{1.12}$$

where $\eta = \eta(t; \omega)$ represents a Wiener process — and $d\eta(t)$ is commonly referred to as "white noise" — while ω labels the particular realization of this random process. The case $\mathbf{g}(\mathbf{X}) = \mathbf{const.}$ is the case of additive noise, while in the case of $\partial \mathbf{g}(\mathbf{X})/\partial \mathbf{X} \neq 0$ we speak of multiplicative noise. The distinction between dt and $d\omega$ in Eq. (1.12) is necessary since, roughly speaking

and following Einstein's treatment of Brownian motion (Einstein, 1905), it is the variance of a Wiener process that is proportional to time and thus $d\eta \sim (dt)^{1/2}$.

In the case of random forcing, we can illustrate the concepts introduced by the simple example of Eqs. (1.10, 1.11) above by the random attractor $\mathcal{A}(\omega)$ (yellow band) of Fig. 1.4. In the figure, $d\eta(t; \omega) = \theta(t)\omega$ is the random process that drives the system (solid black line) and the pullback attraction is depicted by the flow of an arbitrary set $\mathcal{B}$ from "pullback times $t = -\tau_2$ and $t = -\tau_1$ onto the attractor (heavy blue arrows).
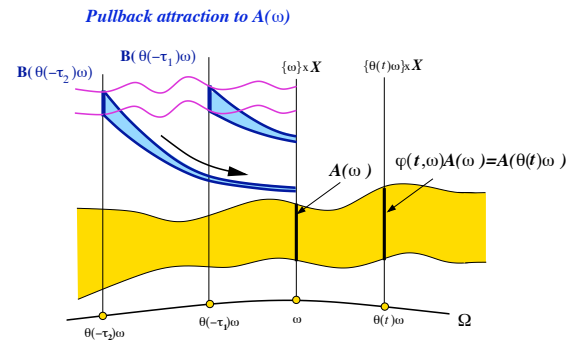

Fig. 1.4. Schematic diagram of a random attractor $\mathcal{A}(\omega)$ and of the pullback attraction to it; here ω labels the particular realization of the random process $\theta(t)\omega$ that drives the system. We illustrate the evolution in time t of the random process $\theta(t)\omega$ (solid black line at the bottom); the random attractor $\mathcal{A}(\omega)$ itself (yellow band in the middle) with the "snapshots" $\mathcal{A}(\omega) = \mathcal{A}(t = 0; \omega)$ and $\mathcal{A}(t; \omega)$ (the two vertical sections, heavy solid); and the flow of an arbitrary set $\mathcal{B}$ from pullback times $t = -\tau_2$ and $t = -\tau_1$ onto the attractor (heavy blue arrows). [After Ghil *et al.* (2008a) with permission from Elsevier.]

More explicitly, we show in Fig. 1.5 four snapshots $\{\mathcal{A}_j(\omega) = \mathcal{A}(\omega; t = t_j) : j = 1, 2, 3, 4\}$ that correspond to the vertical cross-sections (heavy solid) in the attractor of Fig. 1.4; a short video, from which these snapshots are taken, appears as Supplementary Information in Chekroun *et al.* (2011b). These snapshots were calculated for the random attractor $\mathcal{A}(t; \omega)$ of a stochastically perturbed Lorenz system, given

by

$$\mathrm{d}X = Pr(Y - X)\mathrm{d}t + \sigma X\mathrm{d}\eta, \qquad (1.13a)$$

$$\mathrm{d}X = (rX - Y - XZ)\mathrm{d}t + \sigma Y\mathrm{d}\eta \qquad (1.13b)$$

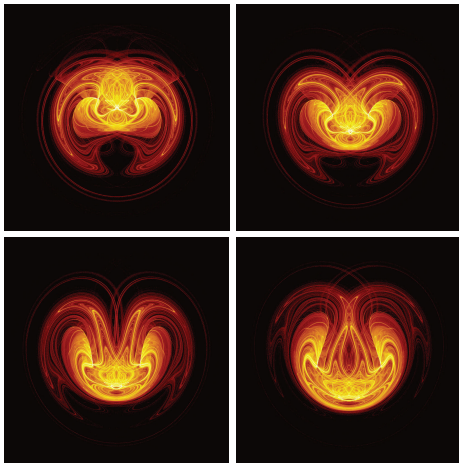$$\mathrm{d}X = (-bZ + XY)\mathrm{d}t + \sigma Z\mathrm{d}\eta. \qquad (1.13c)$$

Fig. 1.5.   Four snapshots of the stochastically perturbed Lorenz (1963) model's random attractor $\mathcal{A}(\omega)$ and the invariant measure $\nu(\omega)$ supported on it. The parameter values are the classical ones — normalized Rayleigh number $r = 28$, Prandtl number $Pr = 10$, and normalized wave number $b = 8/3$ — while the noise intensity is $\sigma = 0.5$ and the time step is $\delta t = 5 \cdot 10^3$. The color bar used is on a log-scale and quantifies the probability to end up in a particular region of phase space; shown is a projection of the 3-D phase space (X, Y, Z) onto the (X, Z)-plane. Notice the complex, interlaced filament structures between highly (yellow) and moderately (red) populated regions. The time interval Δt between two successive snapshots — moving from left to right and from top to bottom — is $\Delta t = 0.0875$. Note that the support of the invariant measure $\nu(t; \omega)$ may change quite abruptly, from time t to time $t + \Delta t$; see the related short video in Chekroun *et al.* (2011b). Weakly populated regions cover an important part of the random attractor and are, in turn, entangled with regions that have near-zero probability (black). [After Chekroun *et al.* (2011b) with permission from Elsevier.]

The parameters r, Pr and b in Eqs. (1.13) have the usual meanings for 2-D thermal convection: $r = R/R_c$ is the Rayleigh number R normalized by its critical value R_c at the onset of convection, Pr is the Prandtl number, and b is a normalized wave number for the most unstable wave at the onset of convection. The noise in

this case is multiplicative: its intensity $\sigma = 0.5$ is multiplied in each one of the three coupled, nonlinear equations above by the corresponding variable X, Y or Z.

To be precise, what is plotted in Fig. 1.5, and in the associated video, is the density of the invariant measure $\nu(\omega)$ supported on the random attractor of the stochastically perturbed Lorenz system governed by Eq. (1.13). This measure indicates the probability of trajectories winding up in a particular region of phase space and it is very highly concentrated on the attractor, as inferred from the huge range of density values: the color bar in the figure is on a logarithmic scale, and extends over more than 10 orders of magnitude. The situation is thus very different from that expected when studying additive noise — in that case, the noise tends to smear out the fine, Cantor-set–like structure of the deterministic, strange attractor and the associated PDF has nonzero-volume support.

It hardly needs saying that additive noise has been studied in climate dynamics much more extensively than the multiplicative sort, for two reasons: (i) it was easier to do so; and (ii) it was suggested by the simple Brownian motion analogy of "weather $\simeq$ water molecules" and "climate $\simeq$ pollen particle," as proposed by Hasselmann (1976). Across the hierarchy of climate models discussed in the previous two sections of this article, however, it is clear that small-and-fast scales of motion do not enter exclusively in an additive manner: they pop up in many, if not all terms of the governing equations, as summarized in Eq. (1.12) above. The insights offered, therefore, by Fig. 1.5 and the video are likely to be of interest across the hierarchy of models, all the way up to and including coupled GCMs and Earth system models.

The invariant measure in Fig. 1.5 exhibits amazing complexity, with fine, very intense filamentation: there is no fuzziness whatsoever in its topological structure, which does evoke the Cantor-set foliation of the deterministic attractor. This fine structure strongly suggests that an

object of vanishing volume supports this measure, i.e. that the random attractor $\mathcal{A}(\omega)$ of system (1.12) has — like the strange attractor of the classical, deterministic version, with $\sigma = 0$ — dimension smaller than 3.

1.5. A Rigorous Definition of Climate Sensitivity

1.5.1. *Equilibrium climate sensitivity*

The usual view of climate sensitivity — as reflected in the work of the Intergovernmental Panel on Climate Change [IPCC: (Houghton *et al.*, 1991; Solomon *et al.*, 2007)] — is that of climate being in equilibrium, in the absence of external perturbations. In the setting of deterministic, autonomous dynamical systems, this view can be described by the change in the position of a fixed point, $\mathbf{X}_0 = \mathbf{X}_0(\mu)$, as a function of a parameter μ.

Going back to Fig. 1.1, we can see how the scalar functional $\bar{T} = \bar{T}\{\mathbf{X}_0(\mu)\}$, namely the global-mean temperature, varies as a function of the fractional change μ of insolation at the top of the atmosphere; here the fixed point $\mathbf{X}_0 = \mathbf{X}_0(\mu)$ is the equilibrium solution $T = T(x; \mu)$ of the EBM given by Eq. (1.2). Climate sensitivity for the present climate is thus simply the partial derivative $\partial\bar{T}/\partial\mu$, i.e. the tangent of the angle γ between the upper branch of Fig. 1.1 and the abscissa. The sensitivity increases, in general, as we approach the bifurcation point (X_0, μ_0) in Eqs. (1.3) or (1.4), and it decreases away from it.
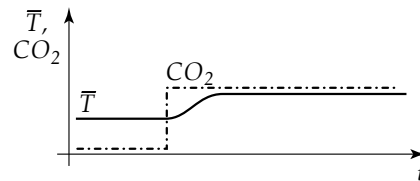
But we have seen in Secs. 1.3 and 1.4 here that internal climate variability can be better described by limit cycles and strange attractors than by fixed points. Moreover, the presence of time-dependent forcing, deterministic as well as stochastic, introduces additional complexities into the proper definition of climate sensitivity.

1.5.2. *Defining climate sensitivity in the presence of variability*

We illustrate in Fig. 1.6 the difference between the ways that a change in a parameter can affect a climate model's behavior in the case of purely periodic solutions vs. the case of equilibrium solutions. One might still think of the former case as the climate of a simpler world, in which ENSO would be purely periodic, rather than irregular. In this case, climate sensitivity can no longer be defined by a single scalar, like $\partial\bar{T}/\partial\mu$, but needs at least three scalars: the sensitivity of the mean temperature along with that of the limit cycle's frequency (or period) and amplitude.

a) Equilibrium sensitivity
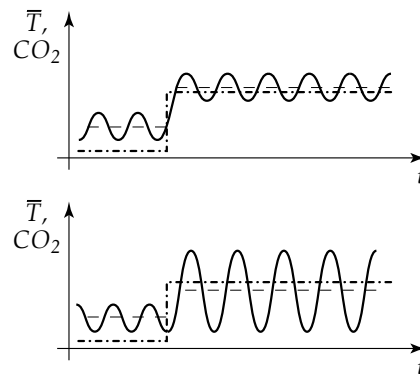

b) Nonequilibrium sensitivity

Fig. 1.6.   Climate sensitivity (a) for an equilibrium model; and (b) for a nonequilibrium, oscillatory model. As a forcing (atmospheric CO_2 concentration, say, dash-dotted line) changes suddenly, global temperature (heavy solid) undergoes a transition: in panel (a) only the mean temperature changes; in panel (b) the mean (shown now as light dashed) adjusts as it does in panel (a), but the amplitude of the oscillation can also decrease, increase or stay the same.

More generally, the setting of non-autonomous and of random dynamical systems, as described in Sec. 1.4, allows one to examine

the interaction of internal climate variability with the forcing, whether natural or anthropogenic, and to provide a definition of climate sensitivity that takes into account the climate systems non-equilibrium behavior and its time-dependent forcing. Such a definition is of the essence in studying systematically the sensitivity of global climate models (GCMs) to the uncertainties in tens of semi-empirical parameters; it will be given here in terms of the response of the appropriate probability densities to changes in the parameters. A comparison with numerical results on parameter dependence for a somewhat simplified GCM (Neelin et al., 2010) goes beyond the scope of this brief overview, and will be given elsewhere.

As an illustration of the more general sensitivity definition that we are proposing, we consider here the case of an infinite-dimensional, but still relatively simple ENSO model. The model is due to Galanti and Tziperman (2000), and its two dependent variables are sea surface temperature T in the eastern Tropical Pacific and thermocline depth h there, as a function of time t:

$$\dot{T} = f(T(t), h(t)), \qquad (1.14\text{a})$$

$$h(t) = g(T, h, F)(t, \tau_1, \tau_2), \qquad (1.14\text{b})$$

$$F(t) = 1 + \epsilon cos(\omega t + \phi). \qquad (1.14\text{c})$$

In Eqs. (1.14), F stands for the seasonal forcing, with period $2\pi/\omega = 12$ months, and all three variables — T, h and F — depend on the time t and the delays τ_1 and τ_2; these delays characterize the traveling times along the Equator of eastward Kelvin and westward Rossby waves. Several authors have studied such delay-differential models of ENSO; see Dijkstra (2005) for a review and Ghil et al. (2008b) for further mathematical details on this type of models. Note that this Galanti-Tziperman model is non-autonomous, because of the seasonal forcing, but it is still deterministic.

The solutions of Eqs. (1.14) exhibit periodic, quasi-periodic and chaotic behavior, as well as frequency locking to the time-dependent, sea-

sonal cycle. Thus, in principle, an infinite number of scalars are required to define the dependence of these solutions on the parameters τ_1 and τ_2; these scalars need to include not just the means of temperature T and depth h, but also their variance and higher-order moments. We have chosen in Fig. 1.7 to represent this dependence for the zeroth, second and fourth moments of $h(t)$; more precisely the plotted quantities are the mean, standard deviation and fourth root of the kurtosis.
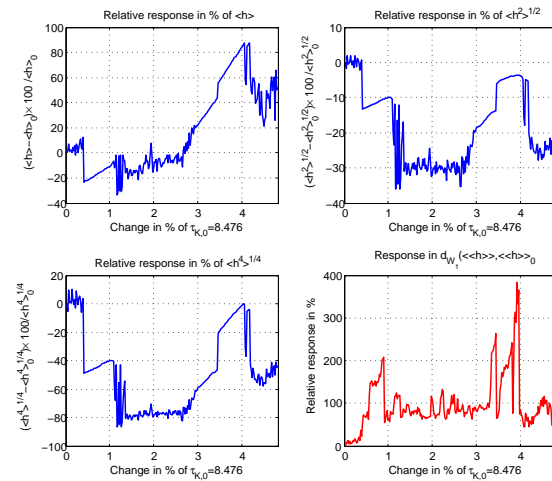

Fig. 1.7.   Relative changes in the statistical properties of the thermocline depth $h(t)$, for the delay-differential ENSO model of Eq. (1.14) and changes of 05% in the delay parameter τ_K associated with the Kelvin wave transit: (a) mean; (b) second moment; (c) fourth moment; and (d) Wasserstein distance d_W. Note intervals of both smooth and rough dependence of the solution on the parameter. [Courtesy of M.D. Chekroun.]

The fourth quantity plotted in Fig. 1.7 is the relative change in *Wasserstein distance* d_W from the same reference solution as for the other three quantities. The Wasserstein distance or "earth movers distance" d_W is the distance between two measures of equal mass on a metric space, i.e., on a space that has a metric attached to it, like an n-dimensional Euclidean space (Dobrushin, 1970). Roughly speaking, d_W represents the total work needed to move the "dirt" (i.e., the measure) from a trench you are digging to

14   M. Ghil

another one you are filling, over the distance be-
tween the two trenches. In general, the shape of
the two trenches and the depth along the trench
— i.e., the support of the measure and its den-
sity — can differ. In the case at hand, the shape
and density of the invariant measure that is be-
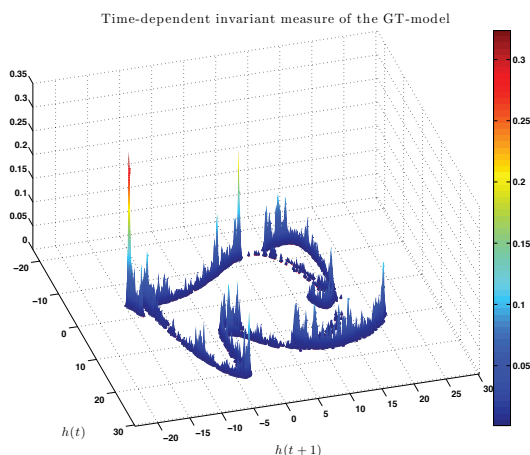ing moved are plotted in Fig. 1.8.

Fig. 1.8.   Time-dependent invariant measure of the
Galanti and Tziperman (2000) model, plotted in an iso-
metric projection with the probability density on the
perpendicular to the plane spanned by the coordinates
$(h(t), h(t+1))$. The time here is in units of years, and
the density is highly concentrated on a very "thin" sup-
port, as for the stochastically perturbed Lorenz model in
Fig. 1.5. [Courtesy of M.D. Chekroun.]

It is quite clear from Fig. 1.7 that intervals
of smooth dependence of the solution on the pa-
rameter alternate with jumps and with intervals
of rough dependence. The jump points are the
same in all four panels of the figure and there
is agreement also in the smooth vs. rough inter-
vals, although the Wasserstein distance in panel
(d) shows some roughness even over intervals in
which the three statistical moments in panels
(a–c) behave smoothly. The latter point is not
too surprising, since d_W contains more informa-
tion than each of the moments.

The very high concentration of probability
density in the peak at the extreme left of Fig. 1.8
might seem surprising but actually agrees with

such a peak in the stochastically perturbed
ENSO model of Timmermann and Jin (2002).
The latter model is based on three ordinary
differential equations, for sea surface tempera-
tures in the eastern and western Tropical Pa-
cific and for thermocline depth, and it was an-
alyzed in detail by Chekroun et al. (2011b).
The corresponding near-singularity in invari-
ant measure on the model's random attrac-
tor evolves regularly in time and thus suggests
that the interaction of deterministic nonlineari-
ties with time-dependent forcing, including even
stochastic perturbations, can help seasonal-to-
interannual prediction, rather than hinder it.
Chekroun et al. (2011a) have taken some inter-
esting steps in exploiting this possibility.

With the results illustrated in Figs. 1.7 and
1.8 in hand, it becomes natural to define climate
sensitivity in the presence of internal variabil-
ity and of time-dependent forcing as the partial
derivative of the Wasserstein distance d_W with
respect to a parameter μ, $\partial d_W / \partial \mu$. Clearly, d_W
has to be defined in turn with respect to the
particular climate whose sensitivity we wish to
evaluate. As usual, it would be awkward, diffi-
cult or even impossible to compute with abso-
lute accuracy the function $d_W = d_W(\mu)$ and its
derivative at $\mu = \mu_0$; but reasonable approxima-
tions should become available shortly, as is the
case already for the calculation of the invariant
measures of models of intermediate complexity.
The definition outlined here for a deterministic
but non-autonomous ENSO model can be gen-
eralized further to the random case, assuming
the existence of the suitable invariant measures.

A complementary approach to climate sensi-
tivity out of equilibrium is the one based on the
fluctuation-dissipation theory of statistical me-
chanics (Leith, 1975; Ghil et al., 1985; Lucarini
and Sarno, 2011). The complementarity arises
from D. Ruelle's extending the many-particle,
statistical-mechanics ideas to low-order dynami-
cal systems subject to certain mathematical con-
ditions on the latter (Ruelle, 1997; Chekroun et
al., 2011b).

We thus expect the theory of random dynamical systems to provide robust tools for studying the parameter dependence of a nonlinear, randomly perturbed system's various "metrics." These metrics — a word used by the climate community in a much broader sense than the standard mathematical term — can include global quantities, like mean temperature or total energy, but also much finer functionals of the state of the system, such as regional temperatures or precipitation. In addition, this theory can help improve prediction of future system properties, by relying on a judicious combination of the history of its slow and fast behavior.

1.6. Concluding Remarks

A complete theory of climate variability, across the entire range of time scales of interest, is still in the future. We have shown, though, that powerful conceptual and numerical tools exist in order to organize the emerging knowledge so far. The approach described herein relies on applying systematically dynamical systems theory, both deterministic and stochastic, across a hierarchy of models, from the simplest toy models to the most detailed, coupled GCMs. This approach has progressed from its first modest steps, taken half-a-century ago, to the analysis of the behavior of atmospheric, oceanic and coupled GCMs over the last two decades. Particularly interesting strides have been taken over the last decade in studying the interaction of the faster time scales with the slower ones, within a genuinely nonlinear framework.

Acknowledgments

References

A. A. Andronov and L. S. Pontryagin (1937) Systèmes grossiers. *Dokl. Akad. Nauk SSSR*, **14**(5), 247–250.

L. Arnold (1998) *Random Dynamical Systems* (Springer-Verlag, New York/Berlin).

V. I. Arnol'd (1983) *Geometric Methods in the Theory of Ordinary Differential Equations* (Springer-Verlag, New York/Berlin), 334 pp.

F. Bryan (1986) High-latitude salinity effects and interhemispheric thermohaline circulations, *Nature*, **323**, 301–304.

M. I. Budyko (1969) The effect of solar radiation variations on the climate of the Earth, *Tellus*, **21**, 611–619.

J. G. Charney *et al.* (1979) *Carbon Dioxide and Climate: A Scientific Assesment* (National Academies Press, Washington, D.C.)

M. D. Chekroun, D. Kondrashov and M. Ghil (2011a) Predicting stochastic systems by noise sampling, and application to the El Niño-Southern Oscillation, *Proc. Natl. Acad. Sci. USA*, **108**(29), 11,7660–11,771, `doi:10.1073/pnas.1015753108`.

M. D. Chekroun, E. Simonnet and M. Ghil (2011b) Stochastic climate dynamics: Random attractors and time-dependent invariant measures, *Physica D*, **240**(21), 1685–1700, `doi:10.1016/j.physd.2011.06.005`.

F. Chen and M. Ghil (1996) Interdecadal variability in a hybrid coupled ocean-atmosphere model, *J. Phys. Oceanogr.*, **26**, 1561–1578.

H. A. Dijkstra (2005) *Nonlinear Physical Oceanography: A Dynamical Systems Approach to the Large-Scale Ocean Circulation and El Niño*, 2nd ed. (Kluwer Acad. Publishers, Dordrecht/Norwell, Mass.) 532 pp.

H. A. Dijkstra and M. Ghil (2005) Low-frequency variability of the large-scale ocean circulation: A dynamical systems approach, *Rev. Geophys.*, **43**, RG3002, `doi:10.1029/2002RG000122`.

R. L. Dobrushin (1970) Prescribing a system of random variables by conditional distributions, *Theor. Prob. Appl.*, **15**, 458–486.

J. L. Doob (1953) *Stochastic Processes* (Wiley, New York).

16   M. Ghil

J.-P. Eckmann and D. Ruelle (1985) Ergodic the-
ory of chaos and strange attractors. *Rev. Mod.
Phys.*, **57**, 617–656 (addendum, *Rev. Mod.
Phys.*, **57**, 1115).

A. Einstein (1905) On the movement of small par-
ticles suspended in a stationary liquid de-
manded by the molecular-kinetic theory of
heat, *Ann. d. Physik (Leipzig)*, **17**, 549 ff.,
reprinted in *Investigations on the Theory of
the Brownian Movement, five articles by A.
Einstein*, Fürth, R. (Ed.) and A. D. Cowper
(transl.) (1956, Dover Publ., New York), 122
pp.

E. Galanti and E. Tziperman (2000) ENSO's phase
locking to the seasonal cycle in the fast-SST,
fast-wave, and mixed-mode regimes, *J. At-
mos. Sci.*, **57**, 2936–2950.

M. Ghil (1976) Climate stability for a Sellers-type
model, *J. Atmos. Sci.*, **33**, 3–20.

M. Ghil(1994) Cryothermodynamics: The chaotic
dynamics of paleoclimate, *Physica D*, **77**, 130–
159.

M. Ghil (2001) Hilbert problems for the geosciences
in the 21st century, *Nonlin. Processes Geo-
phys.*, **8**, 211–222.

M. Ghil, R. Benzi and G. Parisi, Eds. (1985)
*Turbulence and Predictability in Geophysi-
cal Fluid Dynamics and Climate Dynamics*
(North-Holland, Amsterdam), 449 pp.

M. Ghil and S. Childress (1987) *Topics in Geophys-
ical Fluid Dynamics: Atmospheric Dynam-
ics, Dynamo Theory and Climate Dynamics*
(Springer-Verlag, New York/Berlin).

M. Ghil and A. W. Robertson (2000) Solving prob-
lems with GCMs: General circulation models
and their role in the climate modeling hier-
archy, in *General Circulation Model Develop-
ment: Past, Present and Future*, D. Randall
(Ed.), Academic Press, San Diego, pp. 285325.

M. Ghil, A. Mullhaupt and P. Pestiaux (1987) Deep
water formation and Quaternary glaciations,
Climate Dyn., **2**, 1–10.

M. Ghil, M. R. Allen, M. D. Dettinger, K. Ide,
D. Kondrashov, M. E. Mann, A. W. Robert-
son, A. Saunders, Y. Tian, F. Varadi, and P.
Yiou (2002) Advanced spectral methods for
climatic time series, *Rev. Geophys.*, **40**(1), pp.
3.1–3.41, `doi:10.1029/2000RG000092`.

M. Ghil, M. D. Chekroun and E. Simonnet (2008a)
Climate dynamics and fluid mechanics: Nat-
ural variability and related uncertainties,
Physica D, **237**, 2111–2126, `doi:10.1016/j.
physd.2008.03.036`.

M. Ghil, I. Zaliapin and S. Thompson (2008b) A
delay differential model of ENSO variabil-
ity: parametric instability and the distribution
of extremes, *Nonlin. Processes Geophys.*, **15**,
417–433.

J. Guckenheimer and P. Holmes (1983) *Nonlinear
Oscillations, Dynamical Systems and Bifurca-
tions of Vector Fields* (Springer-Verlag, New
York/Berlin) 453 pp.

K. Hasselmann (1976) Stochastic climate models,
Part I: Theory, *Tellus*, **28**, 473–485.

I. M. Held and M. J. Suarez (1974) Simple albedo
feedback models of the ice caps, *Tellus*, **26**,
613–629.

J. T. Houghton, G. J. Jenkins and J. J. Ephraums,
Eds. (1991) *Climate Change, The IPCC Sci-
entific Assessment* (Cambridge Univ. Press,
Cambridge, MA) 365 pp.

E. Kalnay (2003) *Atmospheric Modeling, Data
Assimilation and Predictability* (Cambridge
Univ. Press, Cambridge/London, UK) 341 pp.

R. P. Kennett and L. D. Stott (1991) Abrupt
deep-sea warming, paleoceanographic changes
and benthic extinctions at the end of the
Palaeocene, *Nature*, **353**, 225–229.

F. Ledrappier and L.-S. Young (1988) Entropy for-
mula for random transformations, *Prob. The-
ory Related Fields*, **80**, 217–240.

C. E. Leith (1975) Climate response and fluctuation
dissipation, *J. Atmos. Sci.*, **32**, 2022–2026.

Z.-X. Li, K. Ide, H. Le Treut, and M. Ghil (1997)
Atmospheric radiative equilibria in a simple
column model, *Clim. Dyn.*, **13**, 429–440.

E. N. Lorenz (1963) Deterministic nonperiodic flow,
J. Atmos. Sci., **20**, 130–141.

V. Lucarini and S. Sarno (2011) A statistical me-
chanical approach for the computation of the
climatic response to general forcings, *Nonlin.
Processes Geophys.*, **18**, 7–28, `dpi:10.5194/
npg-18-7-2011`.

J. Marotzke (2000) Abrupt climate change and ther-
mohaline circulation: Mechanisms and pre-
dictability, *Proc. Natl. Acad. Sci. USA*, **97**,
1347–1350.

J. D. Neelin, A. Bracco, H. Luo, J. C. McWilliams
and J. E. Meyerson (2010) Considerations for
parameter optimization and sensitivity in cli-
mate models, *Proc. Natl. Acad. Sci. USA*,
107(50), 21,349–21,354.

G. R. North (1975) Analytical solution to a simple
climate model with diffusive heat transport.
J. Atmos. Sci., **32**, 1301–1307.

G. R. North, R. F. Cahalan and J. A. Coakley, Jr.

A Mathematical Theory of Climate Sensitivity   17

(1981) Energy balance climate models, *Rev. Geophys. Space Phys.*, **19**, 91–121.

V. Ramanathan and J. A. Coakley (1978) Climate modeling through radiative convective models, *Rev. Geophys. Space Phys.*, **16**, 465–489.

D. Ruelle (1997) Application of hyperbolic dynamics to physics: Some problems and conjectures, *Bull. Amer. Math. Soc.*, **41**, 275–278.

D. Ruelle and F. Takens (1971) On the nature of turbulence, *Commun. Math. Phys.*, **20**, 167–192, and **23**, 343–344.

S. H. Schneider and R. E. Dickinson (1974) Climate modeling, *Rev. Geophys. Space Phys.*, **25**, 447–493.

W. D. Sellers (1969) A global climatic model based on the energy balance of the earth-atmosphere system. *J. Appl. Meteor.*, **8**, 392–400.

S. Solomon *et al.*, Eds. (2007) *Climate Change 2007: The Physical Science Basis. Contribution of Working Group I to the Fourth Assessment Report of the IPCC* (Cambridge University Press, 2007)

H. Stommel, H. (1961) Thermohaline convection with two stable regimes of flow, *Tellus*, **13**, 224–230.

A. Timmermann and F.-F. Jin (2002) A nonlinear mechanism for decadal El Niño amplitude changes, *Geophys. Res. Lett.*, **29** (1), 1003, `doi:10.1029/2001GL013369`.